PHYSICAL REVIEW B VOLUME 28, NUMBER 12 15 DECEMBER 1983

Surface-phonon spectroscopy of LiF(001) by inelastic scattering of He atoms: Theory and interpretation of time-of-flight spectra

G. Benedek* and J. P. Toennies
Max-Planck-Institut für Strömungsforschung, Böttingerstrasse 4-8, D-3400 Göttingen, Federal Republic of Germany

R. B. Doak
Bell Laboratories, 600 Mountain Ave., Murray Hill, New Jersey 07974
(Received 17 May 1983)

A distorted-wave theory based on a hard-corrugated-wall potential with a time-dependent modulation (dynamic corrugation) and accurately calculated surface-projected phonon densities is used to calculate the relative amplitudes of time-of-flight spectra. The calculated spectra are compared with measured spectra over a wide range of angles. In general, good agreement is obtained under conditions where final-state resonances with bound states of the atom-surface potential are not expected. When these resonance processes occur, anomalies are found in the measured spectra. The results indicate that single-phonon processes dominate the measured spectra and that under certain conditions bulk modes can affect the spectra. Resonance processes may be useful in enhancing otherwise weak interactions.

I. INTRODUCTION

Recent high-resolution time-of-flight (TOF) spectra of ^{4}He nozzle-beam scattering from alkali-halide surfaces[1-5] have provided the first clear evidence on the dispersion curves of surface acoustic Rayleigh waves (RW's). RW dispersion curves have been measured in LiF(001),[1-4] NaF(001),[2-4] NaCl(001),[5] KCl(001),[2-4] and Ag(111),[6] up to the boundary of the surface Brillouin zone. These results demonstrate that atom beams can, in principle, do for surface phonons the same job that neutrons do for bulk phonons. In these previous papers we have concentrated on an analysis of the kinematic information on phonon dispersion curves. In this paper we discuss the kinematic information by analyzing the amplitudes of the TOF spectra. The TOF spectra normally show, besides a certain number of sharp peaks apparently corresponding to surface phonons, a wealth of diverse features. Some of the more diffuse structures can *a priori* be ascribed to either two- and many-phonon processes or to the scattering from single bulk-phonon states. The role of many-phonon processes has long been considered as an important point to be clarified in the analysis of TOF spectra[7-9] in order to assess the capability of the atom-scattering technique in giving explicit information on surface dynamics.

In this paper we show that the one-phonon scattering reflection coefficient calculated for a hard-corrugated-surface (HCS) model is in general good agreement with the features in the TOF spectra taken at different incident angles. This observation offers a strong argument in favor of the assumption that, for ^{4}He beams at 20 meV, one-phonon processes are by far dominant. It is also found that bulk phonons, having a nonzero displacement in the sagittal plane at the surface, give an appreciable contribution to the differential cross section and, in some cases, even overwhelm the RW phonons. On the other hand, we find that the response of the optical phonons, of either surface or bulk nature, is apparently not resolved in the available TOF spectra, such response being smaller than the theoretical prediction.

From the theoretical point of view this study is an extension with improvements of the earlier calculations of Benedek and Garcia,[10] which were aimed at explaining the few preliminary data published by two of us in 1980.[1] The present systematic comparison between theoretical and experimental spectra for several values of the incidence angle ($\theta_i = 18°-72°$) indicates that the one-phonon approximation is usually quite adequate to describe the inelastic scattering of He from LiF(001). Certain residual discrepancies, occurring for distinct values of the momentum transfer and of θ_i, have been attributed to phonon-assisted bound-state resonances.

The paper is organized in the following way. In the next section we briefly describe the experiment and the way in which the TOF spectra are analyzed. In Sec. III we describe the theoretical method. First the distorted-wave dynamical theory is described. Next the method used to obtain the surface-phonon densities is reviewed. In Sec. IV theoretical TOF spectra are compared with the experiments under kinematical conditions in which no resonances are expected and when resonances may occur. The paper closes with a discussion of the importance of resonances in enhancing special features in TOF spectra.

II. EXPERIMENTAL

The apparatus and the kinematic interpretation of the TOF spectra in terms of surface-phonon dispersion curves has been described in detail in a previous paper.[3] In the

apparatus a highly-collimated ($\Delta\theta=0.2°$ and $\Delta v/v\simeq 0.8\%$) primary He-atom beam of energy $\hbar\omega_i\cong 18.8$ meV is scattered from a LiF(001) crystal along the $\langle 100\rangle$ direction. The incident θ_i and final θ_f angles are constrained by the fixed angle θ_{SD} between source and detector to $\theta_i+\theta_f=\theta_{SD}=90°$. High-resolution time-of-flight spectra were measured over a wide range of incident angles θ_i. Typical measuring times varied from 1 to 6 h.

For the present analysis the TOF spectra were transformed into distributions over momentum transfer ΔK,

$$f_{\Delta K}(\Delta K)=f_t[t(\Delta K)]\frac{dt(\Delta K)}{d\Delta K}\ , \tag{2.1}$$

where t is the flight time from the target to detector and is related directly to the energy gained by the scattered atoms,

$$\hbar\omega=\tfrac{1}{2}ml_{\rm td}^2\left[\frac{1}{t^2}-\frac{1}{t_{\rm el}^2}\right]\ , \tag{2.2}$$

where $l_{\rm td}$ is the target-to-detector distance, $t_{\rm el}$ is the TOF of the elastic peak, and m is the atom mass. $t_{\rm el}$ was measured before and after each experiment by rotating the crystal to the nearest diffraction peak. $\hbar\omega$ is related to the momentum transfer via the kinematical equation,[3]

$$\frac{\omega}{\omega_i}=\left[1+\frac{\Delta K}{K_i}\right]^2\tan^2\theta_i-1\ . \tag{2.3}$$

This relationship is called a scan curve and is plotted in Fig. 1 for LiF $\langle 100\rangle$ for selected values of θ_i over a broad range of momentum transfer including several Brillouin zones (extended-zone plot). The solid periodic curves show the expected measured locations of the RW surface dispersion curves S_1 as well as the Lucas modes S_4 and S_6 for positive (phonon-annihilation) and negative (phonon-creation) values of ω.

The Jacobian in Eq. (2.1) is given by

$$\frac{dt}{d\Delta K}=\frac{-\hbar t_{\rm td}^2}{ml_{\rm td}\sin(\theta_{\rm SD}-\theta_i)}\ . \tag{2.4}$$

We note that as a result of the Jacobian the momentum-transfer distributions are distorted in amplitude compared to the measured TOF spectra. Slow peaks are increased and fast peaks are diminished. As seen from the scan curve (see Fig. 1) we thus expect the intensity of events with small values of ΔK to be enlarged and this explains the apparent increase in noise at the left in the momentum-transfer distributions (see especially Fig. 5). In the momentum-transfer distributions the background signal, which was typically of the order of 20—30%, was subtracted off. The present interpretation of the spectra is based only on a comparison of relative shapes and no attempt is made to carry out an absolute comparison of magnitudes.

III. THEORY

The theory used here is essentially a distorted-wave approximation. In the first subsection we formulate the theory to calculate the one-phonon reflection coefficient. This formulation leads to a separation of the problem into two parts: (1) calculation of the coupling matrix, and (2) calculation of the surface-phonon densities, both of which are discussed below. Because of the one-phonon approximation the kinematics are quite straightforward. The incident atom of mass m, energy $\hbar\omega_i$, and momentum $\hbar\vec{k}_i\equiv\hbar(\vec{K}_i,k_{iz})$ is scattered into a final state of energy $\hbar\omega_f=\hbar(\omega_i+\omega)$ and momentum $\hbar\vec{k}_f\equiv\hbar(\vec{k}_i+\Delta\vec{k})$ within a solid angle $d\Omega$ around the detector direction. Here

$$\hbar\Delta k=\hbar(K_f-K_i,k_{fz}-k_{iz})\equiv\hbar(\Delta\vec{K},\Delta k_z)$$

is the total momentum transfer with k_z the component normal to the surface, and capital letters refer to momenta in the plane of the surface. $\Delta\vec{K}$ equals the phonon wave vector $\vec{Q}$ with respect to the nearest surface reciprocal-lattice vector $\vec{G}$, i.e., $\Delta\vec{K}=\vec{Q}+\vec{G}$, whereas the normal momentum transfer $\hbar\Delta k_z=\hbar(k_{fz}-k_{iz})$ is imparted to the crystal center of mass.

A. One-phonon reflection coefficient and calculation of the atom-scattering dynamical matrix

The one-phonon differential reflection coefficient describes the probability that an atom is scattered into a solid angle $d\Omega$ with gain of energy $\hbar\omega$ and is given by[11]

$$\frac{d^2R^{(1)}}{d\hbar\omega\,d\Omega}=\frac{L^4m^2k_f}{4\pi^2\hbar^4|k_{iz}|}\sum_\alpha P_\alpha\sum_\beta|(\beta|\hat{T}_{\vec{k}_f,\vec{k}_i}|\alpha)|^2$$

$$\times\delta(E_\beta-E_\alpha-\hbar\omega)\ , \tag{3.1}$$

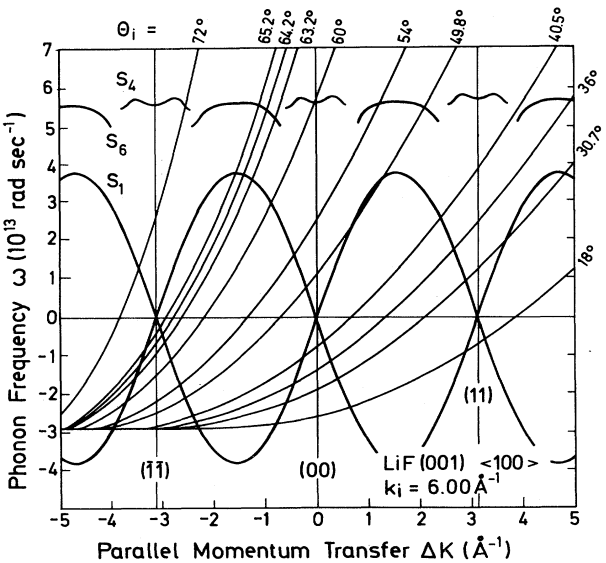

FIG. 1. Scan curves for the inelastic scattering of He from LiF(001) surface for a 90° scattering geometry and for the incidence angles θ_i considered in this work. Intersections with the dispersion curves of RW's (S_1) and optical surface modes with sagittal polarization (S_4 and S_6) indicate possible inelastic processes.

where m is the atom mass and L is a quantization length; $\hat{T}$ is the ordinary transition matrix, and α and β label the crystal states given by different sets of phonon occupation numbers. The prefactor contains the Jacobian for transforming the momentum-coordinate phase-space volume into the angle and energy coordinates as well as flux factors (see below).[12] The factor P_α is the thermal distribution of phonon states α. In order to apply the van Hove transformation, we first use the Fourier representation of the δ function with the result

$$\frac{d^2R^{(1)}}{d\omega d\Omega}=\frac{1}{2\pi}\frac{k_f}{|k_{iz}|}\int_{-\infty}^{+\infty}dt\,e^{-i\omega t}\sum_\alpha P_\alpha\sum_\beta e^{it(E_\beta-E_\alpha)/\hbar}|(\beta|T_{\vec{k}_f,\vec{k}_i}|\alpha)|^2\,, \tag{3.2}$$

where T is $\hat{T}$ divided by the factor $2\pi\hbar^2/mL^2$ and is therefore dimensionless. Following van Hove[13] this can be rewritten to yield[14]

$$\frac{d^2R^{(1)}}{d\omega\,d\Omega}=\frac{1}{2\pi}\frac{k_f}{|k_{iz}|}\int_{-\infty}^{+\infty}dt\,e^{-i\omega t}\langle T_{\vec{k}_f,\vec{k}_i}(0)T^\dagger_{\vec{k}_f,\vec{k}_i}(t)\rangle\,, \tag{3.3}$$

where the time evolution is driven by the free Hamiltonian of the solid only and the brackets $\langle\ldots\rangle$ denote an average over the lattice vibrations and depend on the (surface) temperature T_s. This is also a convenient starting point for deriving efficient approximations of the Debye-Waller factor.[11]

To calculate T we recall that the atom wave function $\psi(\vec{r},t)$ is a mixture of incident and all final-state waves,[15,16]

$$\psi(\vec{r},t)=e^{i\vec{k}_i\cdot\vec{r}-i\omega_i t}+\int d^3k_f A(\vec{k}_f,\vec{k}_i,t)e^{i\vec{k}_f\cdot\vec{r}-i\omega_f t}\,, \tag{3.4}$$

where the time-dependent amplitudes $A(\vec{k}_f,\vec{k}_i,t)$ are related to the T matrix by[16]

$$A(\vec{k}_f,\vec{k}_i,t)=\frac{i\hbar L}{2\pi m}\int_{-\infty}^{t}dt'e^{i\omega t'}T(\vec{k}_f,\vec{k}_i,t')\,. \tag{3.5}$$

Thus, $A(\vec{k}_f,\vec{k}_i,-\infty)=0$, while $A(\vec{k}_f,\vec{k}_i,+\infty)$ is proportional to the Fourier transform of $T(\vec{k}_f,\vec{k}_i,t)$, whose squared modulus gives the scattering cross section.

The scattering amplitudes are determined by the surface boundary conditions. The derivation, however, is complicated by the fact that the surface is oscillating in space and time as a consequence of both static and phonon-induced corrugations. Thus it is convenient to express $T(\vec{k}_f,\vec{k}_i,t)$ as a generalized Fourier transform of the scattering-source function $f(\vec{R},t)$,

$$T(\vec{k}_f,\vec{k}_i,t)=\frac{1}{2L}\int d^2R\,e^{i\Delta\vec{k}\cdot\vec{d}}f(\vec{R},t)\,, \tag{3.6}$$

where $\vec{R}$ denotes the surface position at which the collision occurs, and

$$\vec{d}\equiv(\vec{R},D(\vec{R},t)) \tag{3.7}$$

describes the locus of classical turning points at time t. For a HCS the time-dependent surface $D(\vec{R},t)$ is simply given as a sum of the static corrugation $D_0(\vec{R})$ and of the dynamic corrugation $D_1(\vec{R},t)$ due to lattice vibrations. The HCS model also imposes the simplified boundary condition,

$$\psi(\vec{d},t)=0,\quad\forall\vec{R},t\,. \tag{3.8}$$

Equations (3.2)—(3.4) and (3.6) can now be reexpressed as an integral equation for the source function

$$\int d^2R'dt'M(\vec{R},\vec{R}',t,t')f(\vec{R}',t')=-1,\quad\forall\vec{R},t \tag{3.9}$$

whose kernel

$$M(\vec{R},\vec{R}',t,t')=\frac{i\hbar}{4\pi m}\Theta(t-t')\int d^3k_f e^{i\Delta\vec{k}\cdot(\vec{d}-\vec{d}')}e^{-i\omega(t-t')} \tag{3.10}$$

is the atom Green's function[16] at the surface boundary times

$$(2\pi)^2\exp[i\omega_i(t-t')-i\Delta\vec{k}_i\cdot(\vec{d}-\vec{d}')]\,,$$

and $\Theta(t)$ is the Heaviside unit step function. Note that in Eq. (3.9), $f(\vec{R},t)$ also depends implicitly on $\vec{k}_i$.

At this stage in the calculation we introduce what amounts to the distorted-wave approximation. From Eq. (3.6) it follows that the phonon-modulated potential acts as a small perturbation when $|\Delta k_z D_1(\vec{R},t)|\ll 1$. In this case we can expand M and f in powers of $\Delta k_z D_1$ and keep only the linear terms (one-phonon approximation). With the use of matrix notation we set

$$\underline{M}=\underline{M}_0+\underline{\mu},\quad f=f_0+\varphi \tag{3.11}$$

and write Eq. (3.9) as

$$\underline{M}f=-\underline{\mathbb{1}}\,. \tag{3.12a}$$

$\underline{M}_0$ and f_0 are chosen such that

$$\underline{M}_0 f_0=-\underline{\mathbb{1}}\,. \tag{3.12b}$$

From this we obtain, after neglecting terms in second order in $\Delta k_z D_1$,

$$\varphi=-\underline{M}_0^{-1}\underline{\mu}f_0\,. \tag{3.13}$$

Here $\underline{M}_0$ is given by (3.10) for $\vec{d}=\vec{d}_0=(\vec{R},D_0(\vec{R}))$. From this it follows that

$$\mu(\vec{R},\vec{R}',t,t')=i[D_1(\vec{R},t)-D_1(\vec{R}',t')]L_0(\vec{R},\vec{R}',t,t') , \tag{3.14}$$

with

$$L_0(\vec{R},\vec{R}',t,t')\equiv\frac{i\hbar}{4\pi m}\Theta(t-t') \times\int d^3k_f e^{i\Delta\vec{k}\cdot(\vec{d}_0-\vec{d}_0')-i\omega(t-t')}\Delta k_z . \tag{3.15}$$

The static source function $f_0(\vec{R})$, which can be calculated for the HCS model, is assumed to be known. Thus the one-phonon contributions to $T(\vec{k}_f,\vec{k}_i)$ in (3.6) can be written down explicitly. After extensive rearrangement the correlation function in (3.3) can be written as

$$\langle T_{\vec{k}_f,\vec{k}_i}(0)T^{\dagger}_{\vec{k}_f,\vec{k}_i}(t)\rangle=\frac{1}{4L^2}\int d^2R\,d^2R' e^{i\Delta\vec{k}\cdot(\vec{d}_0-\vec{d}_0')}\int d^2R_1 d^2R_1' dt_1 dt_1' e^{-W(\vec{R}_1)-W(\vec{R}_1')}$$

$$\times Z^*(\vec{R},\vec{R}_1,t-t_1)Z(\vec{R}',\vec{R}_1',t-t_1')\langle D_1(\vec{R}_1,t_1)D_1(\vec{R}_1',t_1')\rangle . \tag{3.16}$$

Equation (3.16) has been written to show explicitly the Debye-Waller factor

$$W(\vec{R})=\tfrac{1}{2}(\Delta k_z)^2\langle D_1(\vec{R},t)D_1(\vec{R},t)\rangle , \tag{3.17}$$

which is a periodic function of $\vec{R}$ but independent of time. The atom-scattering matrix is given by

$$\underline{Z}=\Delta k_z\underline{\tilde{f}}_0-\underline{M}_0^{-1}(\underline{\tilde{L}}_0 f_0)+(\underline{M}_0^{-1}\underline{L}_0)\underline{\tilde{f}}_0 , \tag{3.18}$$

where the vectors f_0 and $\underline{L}_0 f_0$ have been replaced by the diagonal matrices,

$$\underline{\tilde{f}}_0\equiv\delta(\vec{R}-\vec{R}')\delta(t-t')f_0(\vec{R}) , \tag{3.19}$$

$$\underline{\tilde{L}}_0 f_0\equiv\delta(\vec{R}-\vec{R}')\delta(t-t')\int d^2R''dt''L_0(\vec{R},\vec{R}'',t-t'')f_0(\vec{R}'') . \tag{3.20}$$

In the limit of a flat surface ($D_0\to 0$) and small momentum transfer ($\Delta\vec{K}\to 0$) the last two terms in (3.18) give contributions which cancel each other, whereas the first term remains nonzero since $f_0\to 2ik_{iz}$ (*eikonal approximation*).[17] However, the last two terms of (3.18) are expected to yield a small contribution also at nonzero corrugations as in LiF and are omitted in the present calculations. Note that Benedek and Garcia in their previous calculation[10] have neglected these terms on the basis of the incorrect argument that it would involve, at lowest order, only phonons of vanishing parallel momentum.[18] Finally, we note that Eq. (3.16) clearly shows that we have been able to decompose the problem into essentially three factors: (1) the Debye-Waller factor, (2) the atomic-scattering matrix, and (3) the dynamic corrugation, which we discuss next.

The dynamic corrugation $D_1(\vec{R},t)$ which reflects the motion of the surface atoms receives a contribution from all slab normal modes according to

$$D_1(\vec{R},t)=\sum_{\vec{Q},j}\left[\frac{\hbar}{2N_s\omega(\vec{Q},j)}\right]^{1/2}\sum_{\vec{l},\kappa}M_\kappa^{-1/2}\vec{e}_{l_3\kappa}\cdot\frac{\partial D_0(\vec{R})}{\partial\vec{u}(\vec{l},\kappa)}e^{i\vec{Q}\cdot\vec{x}_{\vec{L}}}(b^{\dagger}_{\vec{Q}j}e^{i\omega(\vec{Q},j)t}+b_{\vec{Q}j}e^{-i\omega(\vec{Q},j)t}) , \tag{3.21}$$

where $b^{\dagger}_{\vec{Q}j}$ and $b_{\vec{Q}j}$ are creation and annihilation operators of a phonon with parallel wave vector $\vec{Q}$ and branch index j, $\omega(\vec{Q},j)$ and $\vec{e}_{l_3\kappa}(\vec{Q},j)$ are its frequency and polarization vector, respectively, and $\partial D_0(\vec{R})/\partial\vec{u}(\vec{l},\kappa)$ represents the deformation of the turning-point locus (corrugation in the HCS model) under a unit displacement of the κth ion in the lattice cell of indices $\vec{l}=(\vec{L},l_3)$; $\vec{x}_{\vec{L}}$ are the N_s lattice translations along the surface, and M_κ is the κth ion mass.

With the use of Eqs. (3.16) and (3.21), and the approximation to Eq. (3.18), $\underline{Z}=\Delta k_z\underline{\tilde{f}}_0$, and performing the thermal average, we have finally

$$\frac{d^2R^{(1)}}{d\omega\,d\Omega}=\frac{1}{8\pi^2}\frac{k_f}{|k_{iz}|}\frac{1}{1-e^{-\hbar\omega/k_BT_S}}\sum_{l_3,l_3',\kappa,\kappa',\alpha,\beta}Z^*_{l_3\kappa\alpha}(\Delta\vec{k})Z_{l_3'\kappa'\beta}(\Delta\vec{k})\tilde{\rho}_{l_3\kappa\alpha l_3'\kappa'\beta}(\vec{Q},\omega) , \tag{3.22}$$

where T_s is the surface temperature, $\tilde{\rho}(\vec{Q},\omega)$ is the surface-phonon density matrix,[19] and Z is the dimensionless coupling vector,

$$Z_{l_3\kappa\alpha}(\Delta\vec{k})=\frac{\Delta k_z}{L}\left[\frac{\hbar}{2\omega M_\kappa}\right]^{1/2}\int d^2R\,e^{-W(\vec{R})+i\Delta\vec{k}\cdot\vec{d}_0(\vec{R})}f_0(\vec{R})\frac{\partial D_0(\vec{R})}{\partial u_\alpha(\vec{l},\kappa)} . \tag{3.23}$$

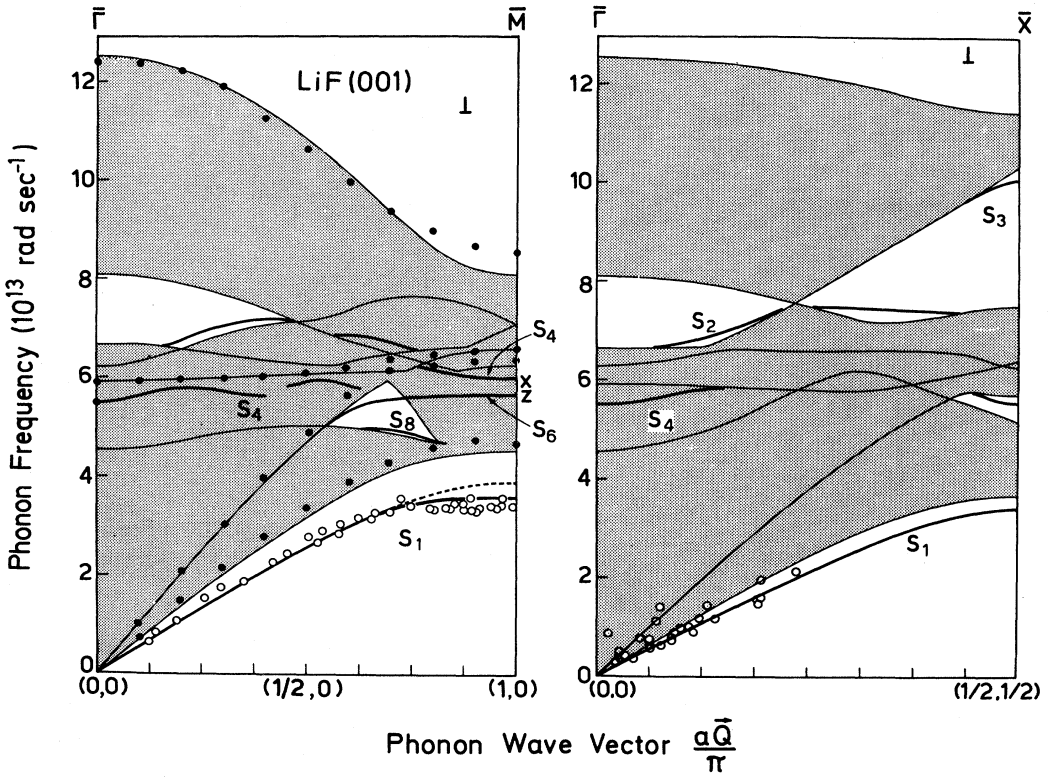

FIG. 2. Calculated surface-phonon dispersion curves of LiF(001) along symmetry directions for sagittal polarization. He-scattering experimental data (○, from Ref. 3) are aligned along the Rayleigh dispersion curve (S_1). Neutron-scattering data (●) corresponding to bulk band edges are taken from Dolling *et al.* (Ref. 30).

The transfer function $\partial D_0(\vec{R})/\partial \vec{u}(\vec{l},\kappa)$ involves, in principle, a microscopic description of the surface potential and its modification under nuclear (core) displacements. For metal and semiconductor surfaces the best way to determine this function would be to carry out an extension of the calculations reported by Hamann[20] for GaAs(110) and Ni(110) $-H(2\times1)$ static surfaces. The Fourier transform in (3.23) tells us that the longer the range of the transfer function, the weaker the response at large $\Delta\vec{K}$. This result, first derived by Armand *et al.*,[21] yields a cutoff for phonon momenta $\vec{Q}$ larger than a critical $\vec{Q}_c$ and has been used to explain some of the anomalies observed in the phonon inelastic scattering of Ne from Ni(111) by Feuerbacher and Willis.[22,23] For closed-shell insulator surfaces like LiF(001) the electron-density perturbation is strongly localized so a much simpler model can be used for the transfer function. We have considered only the effect of ions in the first layer ($l_3=l'_3=\frac{1}{2}$) and taken

$$\frac{\partial D_0(\vec{R})}{\partial \vec{u}(\vec{0},\frac{1}{2},\kappa)}=\begin{cases}(-\partial D_0(\vec{R})/\partial \vec{R},1), & \vec{R}\in A_\kappa\\ \vec{0}, & \vec{R}\notin A_\kappa\end{cases} \tag{3.24}$$

where A_κ is an area surrounding the κth ion in the cell at $\vec{l}=(\vec{0},\frac{1}{2})$, proportional to the square of its ionic radius[24] and such that $\Sigma_\kappa A_\kappa$ is the surface unit-cell area. Thus the dynamical problem is reduced to a calculation of $D_0(\vec{R})$ and $f_0(\vec{R})$. These were obtained from fitting previously measured diffraction amplitudes by means of a method introduced by Garcia.[25]

B. Calculation of surface phonon densities

In this paper the elements of $\tilde{\rho}(\vec{Q},\omega)$ are obtained from a new Green's-function calculation of surface lattice dynamics, the details of which are reported elsewhere.[26,27] These results are based on the Schröder and Nüsslein breathing-shell model[28] (BSM) and room-temperature data corresponding to the experimental conditions. The bulk ($\alpha_\pm$) and surface ($\alpha^s_\pm$) ion polarizabilities are set equal ($\alpha_\pm=\alpha^s_\pm$) and taken from the classical compilation of Tessman, Kahn, and Shockley.[29] This choice of the parameters gives a good fit of both bulk and surface experimental dispersion curves, respectively, obtained from neutron[30] and atom scattering[3] as shown in Fig. 2. Small deviations occur at the $\bar{M}$ point, which have been attributed to different mechanisms including surface elastic relaxation, surface-enhanced anharmonicity, different electronic structure at the surface causing a change in ion polarizabilities[10] and Szigeti charge.[27,31] We are in favor of the polarizability mechanism since a noticeable deviation is observed only in LiF, where at the Brillouin-zone boundary ($\bar{M}$ point) only the polarizable anion is moving in the RW S_1; in NaF and KC1,[32] where the anion—the polarizable

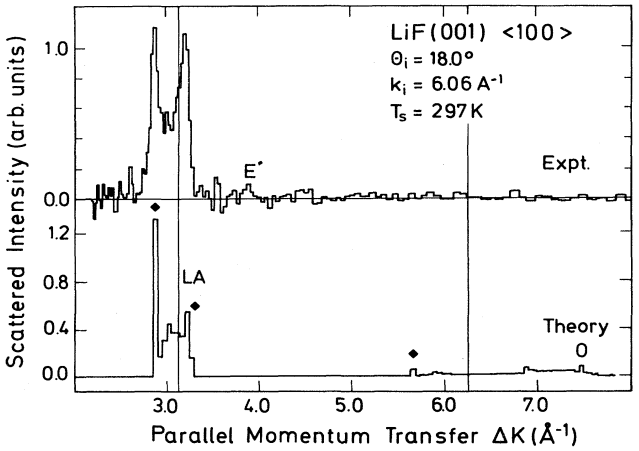

FIG. 3. Experimental TOF spectrum and calculated one-phonon reflection coefficient for scattering of He from LiF(001)⟨100⟩ for $\theta_i = 18.0°$ and $k_i = 6.06$ Å^{-1}. E labels the position of the elastic peak. Theoretical positions of Rayleigh peaks (◆), LA band edge (LA), and optical surface modes (0) are indicated in the calculated spectrum.

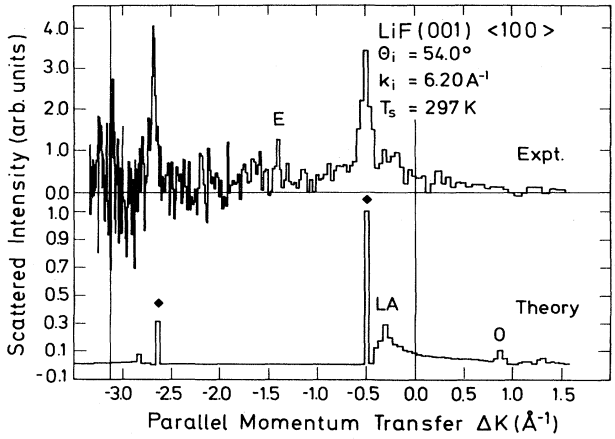

FIG. 5. Same as Fig. 3 for $\theta_i = 54.0°$ and $k_i = 6.20$ Å^{-1}.

object—is at rest, no deviation is found. As shown in Ref. 27 for LiF, if α^s_- is allowed to be larger than α_-—in order to account for the effect of smaller coordination—and both are adjustable, the residual discrepancies at the $\bar{M}$ point can be removed in both bulk and S_1 dispersion curves. Still, we did not use this fitting procedure here since such a refinement is time consuming and, moreover, has a negligible effect on the phonon densities, at least on the scale of the present analysis. We note that previously Schröder's original BSM input data[23] including the surface-polarizability change were used in a preliminary calculation of the one-phonon reflection coefficient.[8]

For planar scattering along ⟨100⟩ only sagittal (⊥) components of $\tilde{\rho}(\vec{Q},\omega)$ with $\vec{Q}=(Q,0,0)$ enter into (3.22). They are calculated for 33 equally spaced values of Q in the irreducible segment $\bar{\Gamma}-\bar{M}$ and 101 values of ω between zero and the maximum crystal frequency. Thus the computational resolution in momentum and frequency is equal to $\Delta Q = 0.05$ Å^{-1} and $\Delta\omega = 0.12\times10^{13}$ rad s^{-1}, respectively. This is close to the experimental resolution and entirely adequate for a significant theory-to-experiment comparison. In order to display the sharp δ functions occurring in $\tilde{\rho}(\vec{Q},\omega)$ at the RW S_1 they have been replaced by equivalent rectangular areas having a width equal to $\Delta\omega$. As a result a RW peak closer than $\Delta\omega$ to the acoustical edge is not resolved from the continuum of the bulk band.

The inelastic spectrum for a given scattering geometry (incidence angle θ_i and final angle $\theta_f = 90° - \theta_i$) involves the set of matrices $\tilde{\rho}(\vec{Q},\omega)$ with ω related to $\vec{Q}$ through the kinematical equation (2.3) (see Fig. 1). Since $\tilde{\rho}(\vec{Q},\omega)$ is known for each $\vec{Q}$ over a discrete frequency mesh its value at the particular ω given by (2.3) is obtained from a linear interpolation. At large θ_i, where the scan curves are rather steep, the chosen mesh of $\vec{Q}$ values becomes relatively coarse, so that some of the spectra for $\theta_i > 60°$ have been evaluated over a double mesh of 65 $\vec{Q}$ values in $\bar{\Gamma}-\bar{M}$, which also have been generated by linear interpolation.

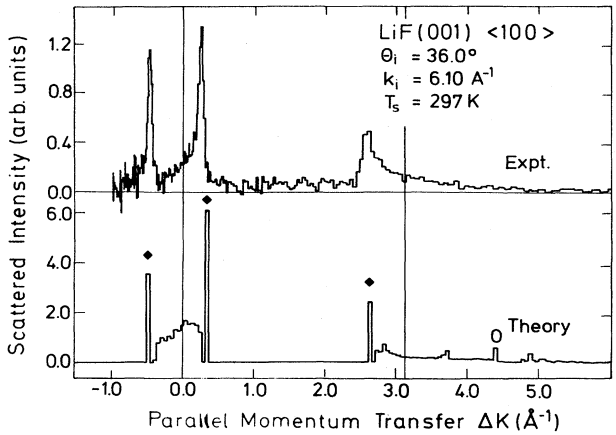

FIG. 4. Same as Fig. 3 for $\theta_i = 36.0°$ and $k_i = 6.10$ Å^{-1}.

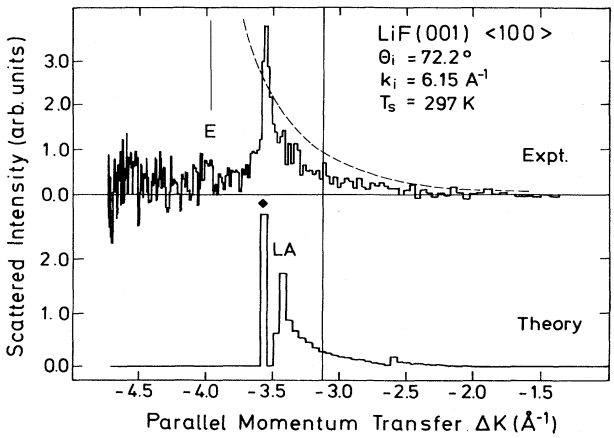

FIG. 6. Same as Fig. 3 for $\theta_i = 72.2°$ and $k_i = 6.15$ Å^{-1}. Bose factor for annihilation processes is represented by the dashed line.

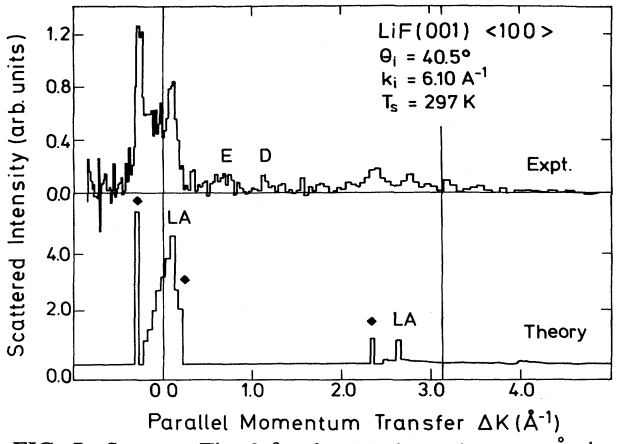

FIG. 7. Same as Fig. 3 for $\theta_i = 40.5°$ and $k_i = 6.10$ Å^{-1}. D labels the diffused diffraction peak, due to the diffraction of atoms with incident velocities different from the nominal velocity.

IV. ANALYSIS OF TOF SPECTRA

In this section we compare the calculated one-phonon reflection coefficient with some selected TOF spectra. Out of the systematic comparison made for LiF(001) over a large number of different incidence angles and documented in Appendix F of Doak's thesis,[4] we have chosen the more interesting and informative spectra. They are divided in two groups. The first group (Figs. 3—8) contains spectra which are not affected by resonances with bound states of the atom-surface potential and are in good agreement with theory. In the second group (Figs. 9—13) we collect some spectra showing clear effects of resonances as predicted from the kinematics and known bound-state energies.[33] In each figure the kinematical parameters θ_i and k_i and the surface temperature are indicated. The vertical lines correspond to $\Delta K = G = (integer) \times 2\pi/a$, where $a = 2.01$ Å is the nearest-neighbor ion distance. Since the experimental integrated intensity is strongly modulated by initial-state resonances[34]—an effect not included in the theory—the spectra are plotted in arbitrary units.

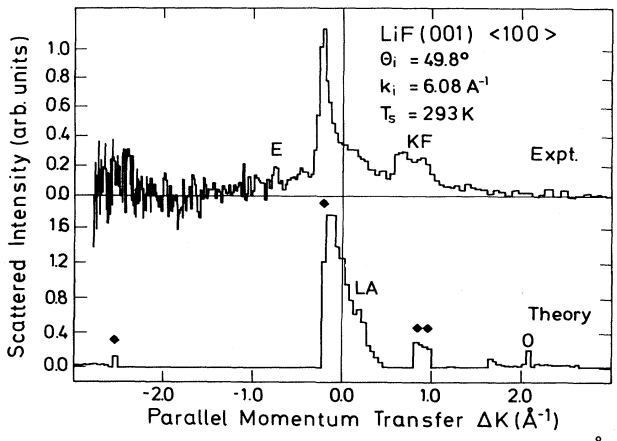

FIG. 8. Same as Fig. 3 for $\theta_i = 49.8°$ and $k_i = 6.08$ Å^{-1}. Broadening effect due to the coalescence of two Rayleigh peaks under KF conditions appears in both experimental and theoretical spectra.

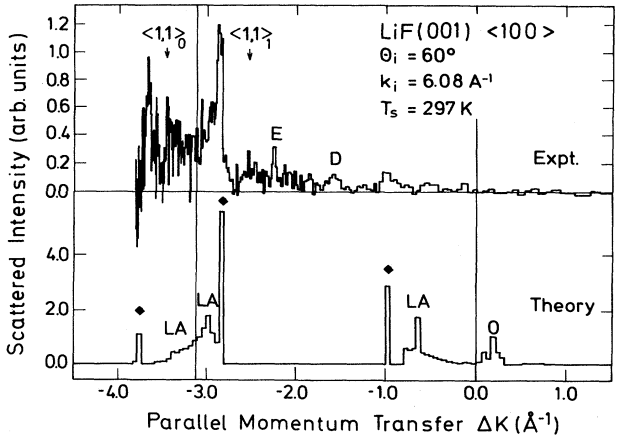

FIG. 9. Same as Fig. 3 for $\theta_i = 60.0°$ and $k_i = 6.08$ Å^{-1}. Additional peaks due to inelastic resonances with the bound states are seen in the experimental spectrum. They are marked by the corresponding G vector (here $\vec{G} = \langle 1,1 \rangle$) and bound-state label ($n = 0, 1, \ldots$).

A. Nonresonant inelastic spectra

Figures 3—6 show four spectra for equally spaced values of θ_i (= 18°, 36°, 54°, and 72°). Inelastic scattering occurs essentially in two regions, corresponding to phonon-creation and -annihilation processes, which, with each new angle, shift to the left by approximately an integer G value. The relative intensities of the different structures change considerably with angle. At the extreme angle $\theta_i = 18°$ phonon-annihilation processes are not resolved from the background, while at the other extreme, $\theta_i = 72°$, only annihilation processes are observed.

At first glance, the calculated spectra appear to be in remarkable agreement with experiment and suggest that a complete interpretation of the TOF spectra should be possible. The sharper experimental peaks correspond quite

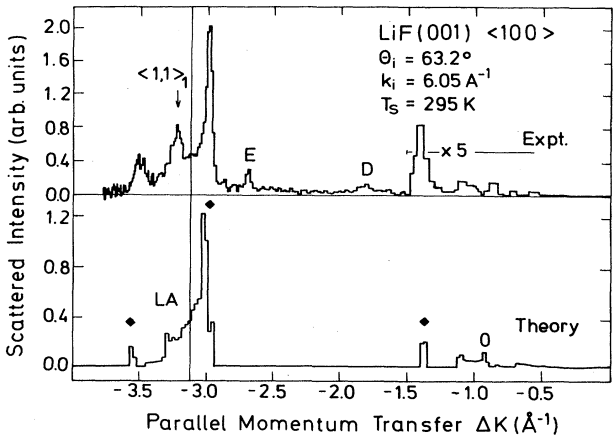

FIG. 10. Same as Figs. 3 and 9 for $\theta_i = 63.2°$ and $k_i = 6.05$ Å^{-1}. Right-hand part of the experimental spectrum has been magnified 5 times: Here the weak structure around $\Delta K = -1$. Å^{-1} is probably significant and in agreement with the calculated features in the optical region.

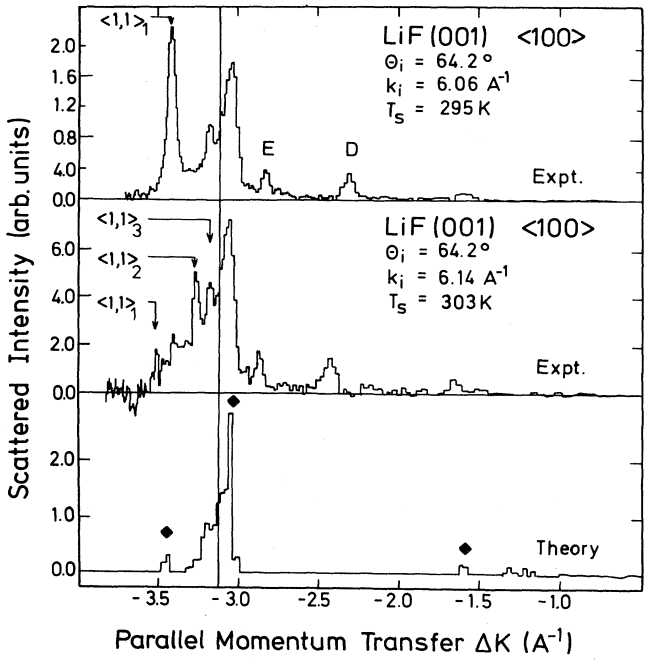

FIG. 11. TOF spectra taken at the same incident angle $\theta_i = 64.2°$ and slightly different incident momentum. Dramatic change in the spectral shape and the large discrepancies with the calculated spectrum are due to the bound-state resonances. For $k_i = 6.06$ Å^{-1} one of the RW peaks is tuned on the $\langle 1,1\rangle_1$ resonance and is strongly enhanced.

well to RW peaks (marked by ◆). Particularly at $\theta_i = 36.0°$ (Fig. 4) the intensities of the three distinct RW peaks are in very good agreement with the predicted intensities. Furthermore, the experimental tails, adjacent to the RW peaks, are seen to reflect quite well the bulk-phonon structures, particularly those arising from the edge of the longitudinal-acoustic (LA) band, which appear on the annihilation side for $\theta_i = 36°$, 54°, and 72° (Figs. 4–6). Also the peak at $\Delta K = 3.2$ Å^{-1} for $\theta_i = 18°$ (Fig. 3), although not well reproduced by theory, originates from the LA

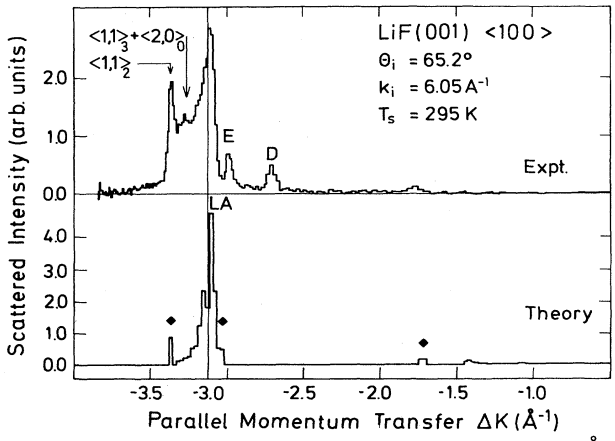

FIG. 12. Same as Fig. 9 for $\theta_i = 65.2°$ and $k_i = 6.05$ Å^{-1}. Here a RW peak is enhanced by the $\langle 1,1\rangle_2$ resonance.

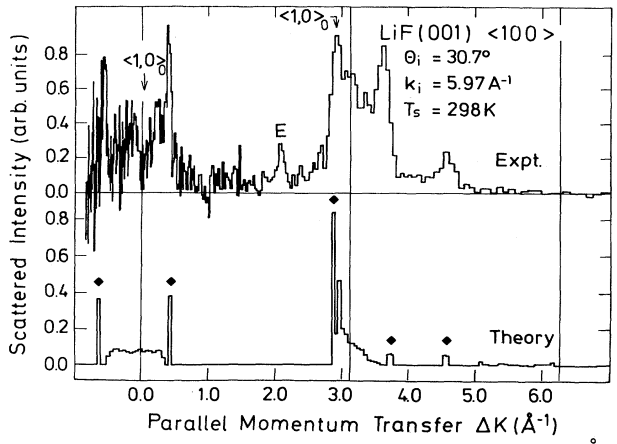

FIG. 13. Same as Fig. 9 for $\theta_i = 30.7°$ and $k_i = 5.97$ Å^{-1}. Here the out-of-plane resonance $\langle 1,0\rangle_0$ yields a reduction of the RW intensity at 3.0 Å^{-1} and a sharp minimum at $\Delta K = 0$.

edge rather than from a RW. This is even more evident in the spectrum at $\theta_i = 40.5°$ (Fig. 7) for the peak at 0.1 Å^{-1}, which is well reproduced by theory. On this side of the specular peak the RW plays a negligible role and is not resolved. This is not surprising if we consider that at long wavelengths the RW penetrates deeply into the solid with a corresponding loss in amplitude, in comparison to the bulk modes.

In Fig. 6, the tail of annihilation processes for $\theta_i = 72°$ is compared with the corresponding Bose factor (broken line). It is seen that the response of the high-energy phonons dies off more rapidly than by the statistical weight.

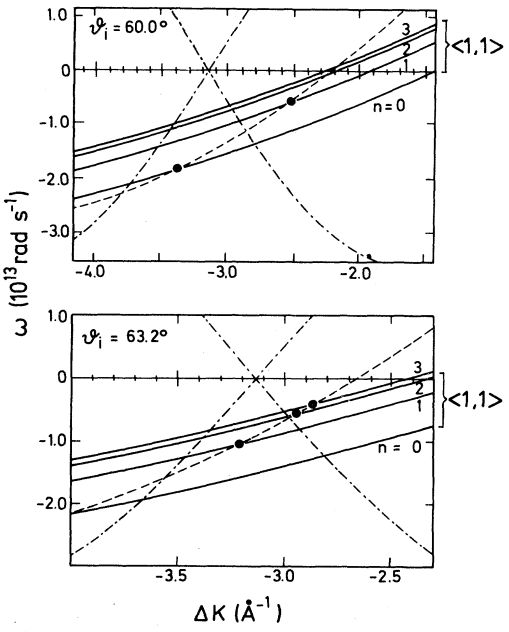

FIG. 14. Bound-state resonance conditions (solid lines) for $\theta_i = 60.0°$ and 63.2°. Intersections with the scan curve (dashed line) give the positions of the inelastic resonances (see Figs. 9 and 10, respectively).

The faster decay indicates an appreciable effect of the phonon density as well as of the coupling mechanism.

The spectrum for $\theta_i = 49.8°$ (Fig. 8) shows the kinematical focusing (KF) effect, occurring when a scan curve is tangent to a surface-phonon dispersion curve.[35] While in angular distributions KF contributes an inverse-square-root singularity, in TOF spectra KF yields a broadening due to the continuum of scattering channels, which are accessible over a nonzero range of momentum transfer. The effect is well simulated by the calculation thanks to the assumed nonzero width of the RW peaks. In this and other spectra theory predicts also a small peak for the sagittal Lucas mode (marked by 0), of which no evidence is found in the present TOF measurements.

B. Effect of resonances

The TOF spectra displayed in Figs. 9–13 ($\theta_i = 60.0°$, 63.2°, 64.2°, 65.2°, and 30.7°) are only in qualitative agreement with theory. However, there are important discrepancies occurring *locally* in the spectra (indicated by arrows). They consist in the appearance of additional peaks, or in the strong amplification of small existing peaks, or in the sharp suppression of a certain spectral region.

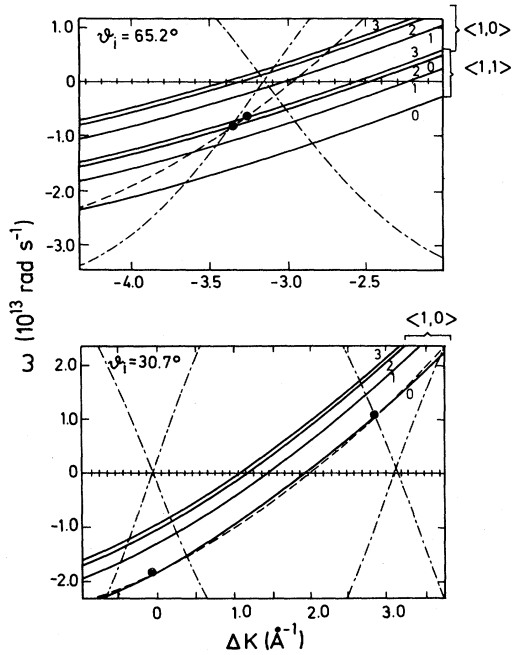

FIG. 16. Same as Fig. 14 for $\theta_i = 65.2°$ (see Fig. 12) and 30.7° (see Fig. 13). In the latter case the intersections with the out-of-plane resonances $\langle 1,0 \rangle_n$ yield minima.

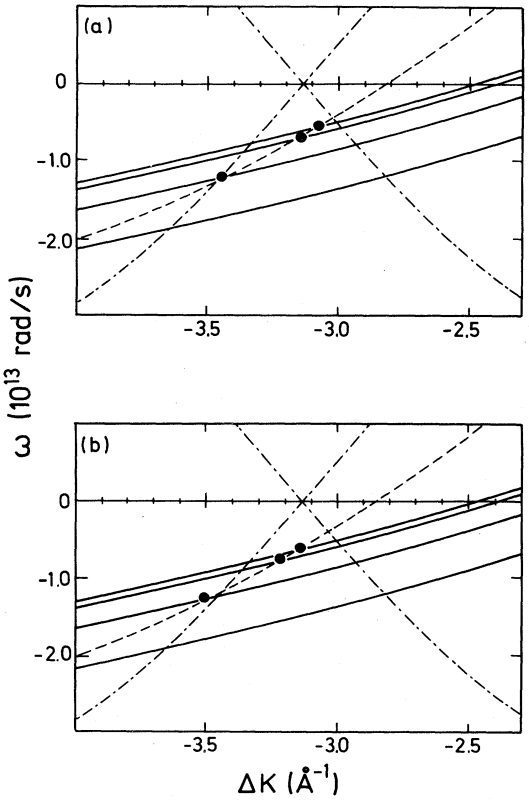

FIG. 15. Same as Fig. 14 for $\theta_i = 64.2°$ with (a) $k_i = 6.06$ Å^{-1} and (b) $k_i = 6.14$ Å^{-1}. Triple intersection of resonance condition, scan curve, and RW dispersion curve occurring in (a) explains the resonance enhancement of the RW peak in Fig. 11.

We propose here an interpretation of these features in terms of phonon-assisted resonances with bound states. The kinematics of these processes has been first described by Cantini, Felcher, and Tatarek.[36] The dynamics of phonon-assisted resonances and their intensities have been investigated[37] and have been reported elsewhere.[38]

In these phonon-assisted resonances the final state, instead of the initial state, can come into resonance with some bound state of energy $-\epsilon_n$ by a change in parallel momentum $\vec{N}$, which is equal to an integral number of reciprocal-lattice vectors. Thus for resonance, energy conservation requires that

$$\omega_i + \omega = \frac{\hbar}{2m}(\vec{K}_i + \Delta\vec{K} + \vec{N})^2 - \frac{1}{\hbar}\epsilon_n \ . \tag{4.1}$$

For planar scattering, the resonance condition (4.1) is represented in the $(\omega, \Delta K)$ plane by a parabola for each $\vec{N}$ and bound-state quantum number n (Figs. 14–16, solid lines). The intersections of such a parabola with the scan curve (dashed line) for given incidence and final angles give energy and momentum of the specific phonon assisting the resonance. The intensity of these phonons in the TOF spectrum is then enhanced or depressed, depending on the phases. The phases appear to depend on whether in-plane or out-of-plane resonances are involved, with in-plane resonances usually leading to maxima and out-of-plane resonances to minima. A rigorous account of the observed behavior, however, requires a careful analysis of the phase shifts and of the Debye-Waller factor along the lines illustrated in Refs. 37 and 38.

As far as kinematics is concerned we see for $\theta_i = 60°$, 63.2°, 64.2°, and 65.2° an excellent correspondence be-

tween the expected in-plane resonances, involving an in-plane reciprocal-lattice vector $\vec{N}=(\sqrt{2}\pi/r_0)\langle 1,1\rangle$ and the observed enhancements. For $\theta_i=60.0°$ (Figs. 9 and 14) the resonance $\langle 1,1\rangle_0$ at -3.4 Å^{-1} yields essentially a strong amplification of the LA edge. The resonance $\langle 1,1\rangle_1$ falls outside the allowed one-phonon region where a small bump occurs at -2.5 Å^{-1}, which can be interpreted as a resonance enhancement of the many-phonon background. Also the spectrum at $\vartheta_i=63.2°$ (Figs. 10 and 14) shows a sharp resonance slightly apart from the LA edge, corresponding to $\vec{N}=(\sqrt{2}\pi/r_0)\langle 1,1\rangle$ with $n=1$.

The most interesting case occurs at $\vartheta_i=64.2°$. We show in Fig. 11 two spectra taken at slightly different incident energy ($k_i=6.06$ and 6.14 Å^{-1}). For $k_i=6.14$ Å^{-1} [Fig. 15(b)] we have three intersections of the scan curve with the resonance curves for $\langle 1,1\rangle_1$, $\langle 1,1\rangle_2$, and $\langle 1,1\rangle_3$. The first resonance, slightly removed from the RW dispersion curve, shows up as a weak enhancement of the many-phonon background, while the other two have their counterpart in the two peaks, appearing in the bulk acoustic region. At $k_i=6.06$ Å^{-1} the resonance $\langle 1,1\rangle_1$ is exactly on top of the RW dispersion curve, producing a dramatic enhancement of the RW peak at $\Delta K=-3.45$ Å^{-1}. This offers a clear example of *resonance-enhanced inelastic scattering*. The spectra at $\vartheta_i=65.2°$ and 30.7° (Figs. 12, 13, and 16) are those which present the major discrepancies. For $\vartheta_i=65.2°$ (Fig. 12) the spectral region -3.40 Å$^{-1}<\Delta K<-3.15$ Å^{-1} is more intense than in the theoretical calculation due to the occurrence of resonance enhancement of the RW for $\langle 1,1\rangle_2$ and of a weaker structure originating from the combined effects of the two resonances $\langle 1,1\rangle_3$ and $\langle 2,0\rangle_0$. For $\theta_i=30.70°$ (Fig. 13) we have the interesting case of sharp depressions in the TOF spectrum produced by the out-of-plane resonances with $\vec{N}=(\sqrt{2}\pi/r_0)\langle 1,0\rangle$ and $n=0$. Actually a minimum is observed at $\Delta\vec{K}\simeq 0$, which has no counterpart in the calculation, and another, on top of the RW at $\Delta K=2.8$ Å^{-1}, produces a sizable reduction of the sharp peak, which theory predicts at about 3 Å^{-1}.

V. CONCLUSIONS

The calculations based on the HCS model for the scattering theory and the BSM surface dynamics are in general good agreement with the measured TOF spectra of ^{4}He, scattered from LiF(001) along the $\langle 100\rangle$ azimuth. This and the smallness of the inelastic scattering suggests that the basic assumption of a distorted-wave treatment is justified. It is clear, however, that the effects of phonon-assisted resonances from bound states have to be incorporated in the theory in order to remove the remaining discrepancies. This refinement along the line followed by Celli, Garcia, and Hutchison[37] for elastic resonances has been reported recently.[38,39] An even more correct treatment, involving the exact close-coupling wave functions for the elastic scattering, which will automatically take into account all resonance effects, is also in preparation.[40] There is also an interesting experimental aspect in the resonance-enhancement effect, when kinematics predicts it in the one-phonon forbidden region (e.g., $\langle 1,1\rangle_n$ in Figs. 9 and 11 for $k_i=6.14$ Å^{-1}). In this case we have an enhancement of the many-phonon background, which makes it become measurable. The comparison with the enhanced one-phonon scattering due to the same resonance (e.g., $\langle 1,1\rangle_1$ in Fig. 11 for $k_i=6.06$ Å^{-1}) would appear to contain important information concerning the many-phonon processes and their intensities relative to one-phonon processes. From Fig. 11 we can argue that a single RW is a stronger scatterer by an order of magnitude than the many-phonon states nearby. This gives further support to the one-phonon interpretation of the data.

Another important question concerns the possible effect of the softness of the potential in the direction normal to the surface. Soft potentials such as the Lennard-Jones potential have been used in the past, for example, in the framework of the distorted-wave Born approximation.[41] It was found that the softer the potential, the smaller the coupling to RW's compared to the coupling to bulk LA waves because the coupling constants $\vec{Z}_{l_3\kappa}(\Delta\vec{k})$ turn out to be proportional to the matrix element between atom incident and final states of

$$\left\langle -i\,\Delta\vec{K}, \frac{\partial}{\partial z}\right| V_{\kappa,\Delta\vec{K}}(z+al_3)\,,$$

where $V_{\kappa,\Delta\vec{K}}(z+al_3)$ is the two-dimensional Fourier transform of the two-body potential between He and the ion at the site $(\vec{L},l_3,\kappa)$. Therefore, using a potential with a disposable softness parameter, one should be able to estimate the softness from the observed amplitude ratio of the LA-mode peak to the RW peak.[42] Even if this procedure indicates that the softness of the surface potential has an effect, the present study demonstrates that the HCS model is also able to reproduce correctly the amplitudes of LA modes thanks to the fact that the relevant information on the surface potential has been incorporated in the theory through the static source function $f_0(\vec{R})$ and the fitted static corrugation. Thus in the HCS model we are using an effective corrugation, which is known to reproduce the rainbow scattering intensities quite well. These considerations do not mean that the choice of the potential would not have other effects. For instance the prediction of detectable optical Lucas-mode intensities, which have not yet been seen with certainty in the experiments, might be a consequence of too localized an interaction. A soft potential would probably decrease the coupling to optical modes. To pursue this matter further, it would be desirable to have experimental results for optical modes. Resonance-enhanced scattering might provide a way to amplify the response of optical surface modes to He atoms. We are, at present, exploring this possibility, which would hopefully extend the area of investigation of surface dynamics by atom scattering to the whole spectrum of surface phonons.

ACKNOWLEDGMENTS

G. Benedek acknowledges several illuminating discussions with Professor Vittorio Celli (University of Virginia) and is grateful for the kind hospitality he enjoyed at the

Max-Planck-Institut für Strömungsforschung in Göttingen. He also thanks N. Garcia (Universidad Autonoma, Madrid), with whom he published the first investigation of the inelastic scattering from a HCS (Ref. 18), for useful discussions. B. Doak is grateful to the Deutscher Akademischer Austauschdienst for a fellowship and the Deutsche Forschungsgemeinschaft through the Sonderforschungsbereich 126 for a position.

*Permanent address: Gruppo Nazionale di Struttura della Materia del Consiglio Nazionale delle Ricerche, I-20133 Milano, Italy and Dipartimento di Fisica dell'Università degli Studi di Milano, Via Celoria 16, I-20133 Milano, Italy.

[1]G. Brusdeylins, R. B. Doak, and J. P. Toennies, Phys. Rev. Lett. 44, 1417 (1980); 46, 437 (1981).

[2]R. B. Doak and J. P. Toennies, Surf. Sci. 117, 1 (1982).

[3]G. Brusdeylins, R. B. Doak, and J. P. Toennies, Phys. Rev. B 27, 3662 (1983).

[4]R. B. Doak, thesis, Massachusetts Institute of Technology, 1981 (unpublished); Max-Planck-Institut für Strömungsforschung, Göttingen, Bericht 14/1981 (unpublished).

[5]G. Benedek, G. Brusdeylins, R. B. Doak, J. G. Skofronick, and J. P. Toennies, Phys. Rev. B 28, 2104 (1983).

[6]R. B. Doak, U. Harten, and J. P. Toennies, Phys. Rev. Lett. 51, 578 (1983).

[7]Y. W. Lin and J. Wolken, Jr., J. Chem. Phys. 65, 2634 (1976); 67, 1292 (1977).

[8]J. H. Weare, J. Chem. Phys. 61, 2900 (1974).

[9]H. D. Meyer, Surf. Sci. 104, 117 (1981).

[10]G. Benedek and V. Garcia, Surf. Sci. 103, L143 (1981); Le Vide, Les Couches Minces Suppl. 201, 818 (1980).

[11]A. C. Levi and H. Suhl, Surf. Sci. 88, 221 (1979).

[12]H. Schiff, *Quantum Mechanics,* 3rd ed. (McGraw-Hill, New York, 1966), p. 286.

[13]L. van Hove, Phys. Rev. 95, 249 (1954).

[14]J. R. Manson and V. Celli, Surf. Sci. 24, 495 (1971). This work is based on the distorted-wave Born approximation. The theory of inelastic processes in the eikonal approximation for a HCS is presented in A. C. Levi, Nuovo Cimento B 54, 357 (1979).

[15]Here we work in direct space and time coordinates as is also done in G. Benedek and N. Garcia, Surf. Sci. 80, 543 (1979), with the use of different and more standard notations.

[16]E. N. Economou, *Green's Functions in Quantum Physics* (Springer, Berlin, 1979).

[17]V. Garibaldi, A. C. Levi, R. Spadacini, and G. E. Tommei, Surf. Sci. 48, 649 (1975).

[18]G. Benedek and N. Garcia, Surf. Sci. 80, 543 (1979); 103, L143 (1981).

[19]G. Benedek, Surf. Sci. 61, 603 (1976).

[20]D. R. Hamann, Phys. Rev. Lett. 46, 1227 (1981).

[21]G. Armand and J. R. Manson, Surf. Sci. 80, 532 (1979).

[22]B. Feuerbacher and R. F. Willis, Phys. Rev. Lett. 47, 526 (1981).

[23]A. Bortolani, A. Franchini, F. Nizzoli, G. Santoro, G. Benedek, and V. Celli, Surf. Sci. 128, 249 (1983).

[24]F. Fumi and M. P. Tosi, J. Phys. Chem. Solids 25, 31 (1964); 25, 45 (1964).

[25]N. Garcia, J. Chem. Phys. 67, 897 (1977).

[26]G. Benedek and L. Miglio, in *Ab-Initio Calculation of Phonon Spectra,* edited by J. T. Devreese, V. E. van Doren, and P. E. van Camp (Plenum, New York, 1982), p. 215.

[27]G. Benedek, G. P. Brivio, L. Miglio, and V. R. Velasso, Phys. Rev. B 26, 497 (1982).

[28]U. Schröder and V. Nüsslein, Phys. Status Solidi 21, 309 (1967).

[29]J. R. Tessmann, A. H. Kahn, and W. Shockley, Phys. Rev. 92, 820 (1953).

[30]G. Dolling, H. G. Smith, R. M. Nicklow, P. R. Vijayaraghavan, and M. K. Wilkinson, Phys. Rev. 153, 983 (1967).

[31]See also the discussion in J. P. Toennies, Phys. Scr. T1, 89 (1982), and in Ref. 3.

[32]G. Benedek, G. Brusdeylins, R. B. Doak, and J. P. Toennies, J. Phys. (Paris) Colloq. 42, C6-793 (1981).

[33]G. Derry, D. Wesner, S. V. Krishnaswamy, and D. R. Frankl, Surf. Sci. 74, 245 (1978).

[34]G. Brusdeylins, R. B. Doak, and J. P. Toennies, J. Chem. Phys. 75, 1784 (1981).

[35]G. Benedek, Phys. Rev. Lett. 35, 234 (1975).

[36]P. Cantini, G. P. Felcher, and R. Tatarek, Phys. Rev. Lett. 37, 606 (1976).

[37]V. Celli, N. Garcia, and J. Hutchison, Surf. Sci. 87, 112 (1979).

[38]D. Evans, V. Celli, G. Benedek, R. B. Doak, and J. P. Toennies, Phys. Rev. Lett. 50, 1854 (1983).

[39]V. Celli, D. Evans, and G. Benedek, Europhysics Conference Abstracts 6A, 100 (1982).

[40]D. Eichenauer and J. P. Toennies (unpublished).

[41]G. Benedek and G. Seriani, Jpn. J. Appl. Phys. Suppl. 2, Pt. 2, 545 (1974).

[42]G. Benedek and L. Miglio, Z. Phys. B 50, 93 (1983).